Multiuser Correlation and Sum-Rate in Outdoor Measured Massive MIMO Channels

Karstensen, Anders; Nielsen, Jesper Ødum; Eggers, Patrick Claus Friedrich; De Carvalho, Elisabeth; Pedersen, Gert Frølund; Alm, Martin; Steinbock, Gerhard

Published in:
I E E E Antennas and Wireless Propagation Letters

DOI (link to publication from Publisher):
10.1109/LAWP.2020.2969496

Publication date:
2020

Document Version
Accepted author manuscript, peer reviewed version

Multi-User Correlation and Sum-Rate in Outdoor Measured Massive MIMO Channels

Anders Karstensen, Jesper Ø. Nielsen, Patrick C. F Eggers, Elisabeth De Carvalho, Gert F. Pedersen, Martin Alm, Gerhard Steinböck

***Abstract*—This paper analyses the impact of inter-user distance and angular separation on the channel correlation and achievable sum-rate for a massive multiple-input multiple-output system in non line of sight conditions. The investigation is based on outdoor measurements on a channel sounding system capturing the dynamic channel of two user arrays. The paper analyses correlation and sum-rate with varying inter-user distance and angular separation of dominant beams towards the users. A large span of correlation and sum-rate values are found across the range of distances and angular separation. The investigation shows a moderate link between inter-user distance and correlation, but a strong impact on correlation is found only for low angular separation of the users. The results of this non line of sight (NLOS) scenario suggest that a distance based criteria alone is not sufficient to accurately model shared clusters and correlation.**

***Index Terms*—Massive-MIMO, multi-user consistency, measured channels, sum-rate.**

I. Introduction

MASSIVE MIMO (Multiple-Input Multiple-Output) have in the recent years gained a lot of traction as the technology has a large potential for significant increase in throughput and energy efficiency [1] [2] [3]. Massive MIMO systems are expected to consist of base station arrays with tens or hundreds of antenna elements to serve multiple users in the same time and frequency resources [4]. With a large enough number of antennas, the channels towards separate users become increasingly orthogonal, known as favourable propagation [5]. The potential capacity gain of massive MIMO has been observed in both theory and by experiments, but measurements also displays propagation characteristics like non-stationarity, spatial correlation and inter-user correlation that can limit the performance of massive MIMO [6] [7] [8]. When the user channels become correlated, orthogonality and favourable propagation no longer holds, and can reduce channel capacity [9] [10]. If these characteristics are not accurately implemented in channel models used in massive MIMO with multiple users, the simulated capacity could be overly optimistic. Specifically, a distance criteria is often assumed and used to implement the number of shared clusters like in the Quadriga extension [11] or more indirectly by the visibility regions in COST2100 [12].

Anders Karstensen, Jesper Ø. Nielsen, Patrick C. F. Eggers, Elisabeth de Carvalho and Gert F. Pedersen are with the Department of Electronic Systems, Aalborg University, Denmark.

Martin Alm and Gerhard Steinöck are with Huawei Technologies Sweden AB.

This paper will analyse a set of measurements dominantly in NLOS conditions to investigate the impact of inter-user distance and angular separation of users on the user channel correlation as well as on the sum-rate capacity using the maximum ratio transmission and zero-forcing precoders.

II. Measurements

An outdoor measurement campaign was designed around the Aalborg University Campus at Frederik Bajers Vej in Aalborg, Denmark. The area consists of multiple two story buildings with roads, paths and some smaller green areas in between them. A map of the area is depicted in Fig. 1, with the location of the base station (BS) in yellow, and the measurement tracks of the mobile stations (MS) 1 and 2 in blue and red respectively. Tracks were measured simultaneously in pairs with MS1 and MS2 namely A1 and A2, B1 and B2, C1 and C2 as well as D1 and D2. MS1 did multiple measurements that back to back construct the long tracks, while MS2 repeated the same short track until MS1 completed the longer track.

At the end of the area is a taller building with a balcony on the fourth floor where the BS array was located. The two MS arrays where moving simultaneously on the ground in between the two story buildings. Except for the very beginning (left) of A1 track in Fig. 1, there was no line of sight (LOS) between the base station and mobile stations. The distance from the BS to the centre of the open square/park is about 90 metres.

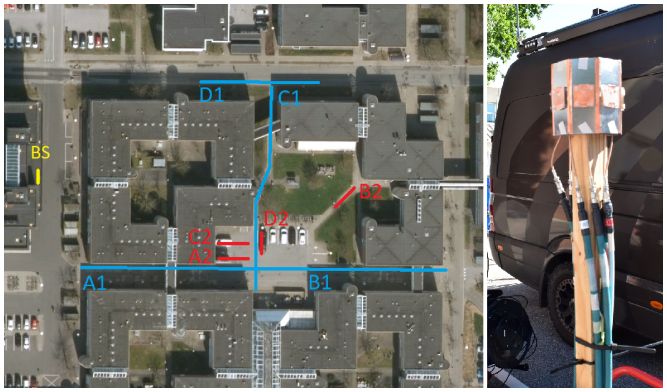

Fig. 1. Map of the measurement area, with location of BS and MS tracks for users 1 and 2 in blue and red respectively. Aerial photo by Agency for Datasupply and efficiency, October 2019 [13]. On the right is a photo of one of the two circular MS arrays.

A. Array configurations

The massive Rx array is configured as two stacked uniform linear arrays (ULAs) of 64 Vivaldi elements [14] each. The array is grouped into 8 modules of 16 elements due to the fast switching structure, which is detailed in Sec. II-B. Element separation is 5 cm, or 0.58 λ at 3.5 GHz, which makes each ULA 3.2 m wide. The in-array measured half power beamwidth of the Vivaldi elements are 99.5° and 34.5° in azimuth and elevation respectively. The array centre was about 16.1 m above ground level. A photo of the stacked BS array in this configuration can be found in [15], Fig. 2.

The two identical Tx arrays are both configured as uniform circular arrays (UCAs) with 8 patch elements each. Each element has a measured half power beamwidth of 75° in azimuth and 55° in elevation. The array was designed with an element separation of 0.46 λ to allow phased processing. The two arrays were mounted on two identical trolleys to be pushed by a person during measurements, one MS array is depicted in Fig. 1 (right). The array centres were at a height of 167 cm above the ground.

B. Mesurement equipment

The measurement campaign was using the correlation based AAU channel sounder [15]. A bandwidth of 100 MHz was measured around the carrier frequency of 3.5 GHz. The sounder has 8 fully parallel receivers (BS) and 16 fully parallel transmitters (8 on each of the two MS). The 8 receive channels are each connected to a 1:16 switch such that a total of 128 elements can be measured semi-simultaneously. With the fast switching, a snapshot of the full 128×16 MIMO channel is recorded in 1.31 ms. Measurements are recorded in 15 second blocks where 900 snapshots are recorded at a rate of 60 Hz, enough to support Nyquist sampling rate at walking speed for both user arrays.

C. Measured data points

A total of 21 measurements of 15 seconds and 900 snapshots each, have been analysed for correlation, directional overlap from BS, and the inter-user distance as well as sum-rate capacity. The 21 measurements of $T = 900$ snapshots each, provides 18900 pairs of user locations across the measurement area. The two users' start and stop positions of each 15 second measurement are known with centimetre accuracy. The positions in between start and stop are interpolated assuming a constant walking speed during the 15 seconds.

III. Data analysis

The eight elements at each user array are summed to emulate $K = 2$ omnidirectional user terminals, and a module of $M = 16$ base station elements are used such that the number of users to BS elements ratio is 1:8. Before analysis the channels are normalized to the average power over snapshots and elements of the array to maintain the difference among elements and users:

$$\mathbf{h}_k(t) = \frac{\mathbf{h}_k^{\text{raw}}(t)\sqrt{MKT}}{\sqrt{\sum_{t=1}^{T}\sum_{k=1}^{K}||\mathbf{h}_k^{\text{raw}}(t)||^2}} \tag{1}$$

where $\mathbf{h}_k(t) \in \mathbb{C}^{M\times 1}$ is the channel vector of M base station antennas towards the k^{th} user at snapshot t.

1) User channel correlation: The correlation between the two users is measured by the normalized scalar product:

$$\rho_{ij} = \frac{\sum_t |\mathbf{h}_i^*(t)\mathbf{h}_j(t)|}{\sqrt{\sum_{t_1}||\mathbf{h}_i(t_1)||^2}\cdot\sqrt{\sum_{t_2}||\mathbf{h}_j(t_2)||^2}} \tag{2}$$

where $()^*$ denotes the complex conjugate transpose and i and j denotes user 1 and 2 respectively. Equation 2 is used for single snapshot case, as well as averaging over multiple snapshots.

2) Main beam separation: Narrowband beam scanning is performed at the base station array to determine the direction of the strongest beam/direction for each user. The angular difference between the two main beams (MB_Δ) is calculated as:

$$\text{MB}_\Delta = |\text{MB}_{\text{MS1}} - \text{MB}_{\text{MS2}}| \tag{3}$$

The main beam is the direction of arrival (DOA) with maximum power from the base station side using narrowband beam scanning towards each user by the Bartlett beamformer [16]: $\text{DOA}(\theta) = a^*(\theta)\hat{R}a(\theta)$

where $a(\theta)$ is the measured complex vector of array element gains in the direction θ and $\hat{R}$ is the estimated covariance matrix:

$$\hat{R} = \frac{1}{T}\sum_{t=1}^{T}\mathbf{h}_k^*(t)\mathbf{h}_k(t) \tag{4}$$

A. Precoding

Maximum ratio transmission (MRT) and zero forcing (ZF) precoders [17] are used to evaluate the sum-rate capacity for the two users. MRT, similar to matched filter, maximises power for each user but does not consider interference. ZF attempts to cancel interference from other users, and will outperform MRT in highly correlated channels.

Both precoders utilizes the actual channel, and perfect channel state information (CSI) is assumed. The SNR is kept at 10 dB for all sum-rate calculations. For power allocation, the water filling algorithm is applied, which is optimal for ZF and sub-optimal for MRT [18]. Power allocation is carried out with the code provided by Björnson *et al* [19]. Ageing CSI, and different SNR ranges can impact the precoders differently [17] [20], but this is out of the scope of this investigation. In case of averaged results, the mean of N single snapshot sum-rates are used.

IV. Results

The inter-user distance is measured by a single straight line between the two users. The correlation values are plotted against the inter-user distances in Fig. 2 along with the mean and the 10 and 90 percentile values in black and blue respectively. This figure and the following figures contain the results of all measurement tracks, the 18900 pairs of user locations. The mean and percentiles are calculated based on 1 m wide bins of the raw data points. The mean correlation has some local variations, but the larger trend is a slowly decreasing correlation with increasing inter-user distance. A simple linear fit on the data points indicate a correlation reduction of 0.0064 per meter increase in user distance. There is however a large span of correlation values compared to the mean. The difference between the 10 and 90th percentile is on average 0.35, but the gap decreases with increasing distance similar to the mean correlation.

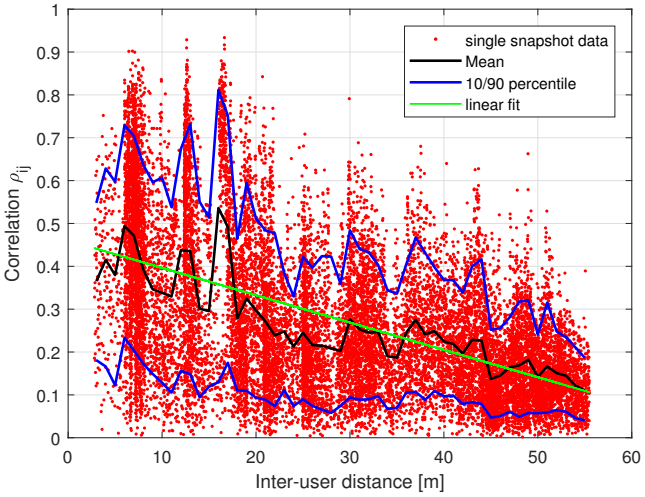

Fig. 2. Inter-user distance vs correlation. Instantaneous samples and mean and 10/90 percentile lines.

The correlation values are plotted against the MB_Δ in Fig. 3. There is a strong link between beam separation and mean correlation for MB_Δ below about 15° and a weaker link for higher angular separation. The mean correlation drops from 0.6 to about 0.25 in the first 15°, and only drops down to about 0.15 in the remaining region (excluding the sparse samples around 80°). The beamforming beam-width of the 16 element array is about 8°. The equivalent figure for a 64 element array with much narrower beam, produces a very similar trend of the mean correlation with strong decrease until about 15°.

The correlation values are plotted against the sum-rates of the ZF and MRT precoders in Fig. 4. Both the correlation and sum-rate in this figure is based on 18 snapshot averages (approximately 2 λ user movement). The MRT precoder shows a very clear link to the channel correlation to achieve a certain sum-rate while the mean sum-rate of the ZF precoder is generally much less dependant on the correlation values.

MRT sum-rates are plotted against inter-user distance in Fig. 5. The mean sum-rate is very similar but inverted shape compared with the mean correlation in Fig. 2. These are similar as the sum-rates and correlation have the very strong

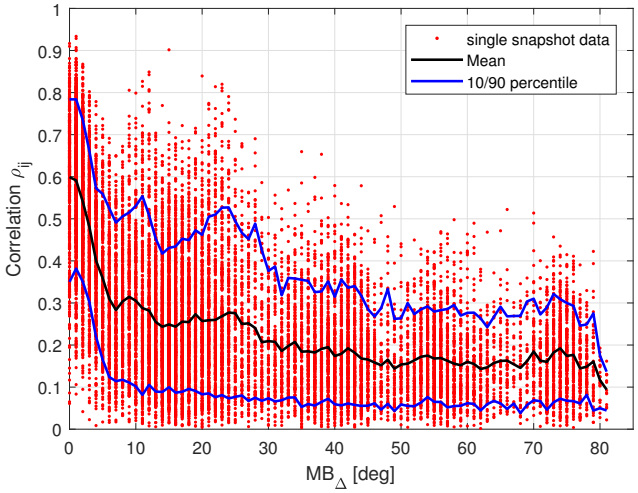

Fig. 3. Angular separation of main beam vs correlation.

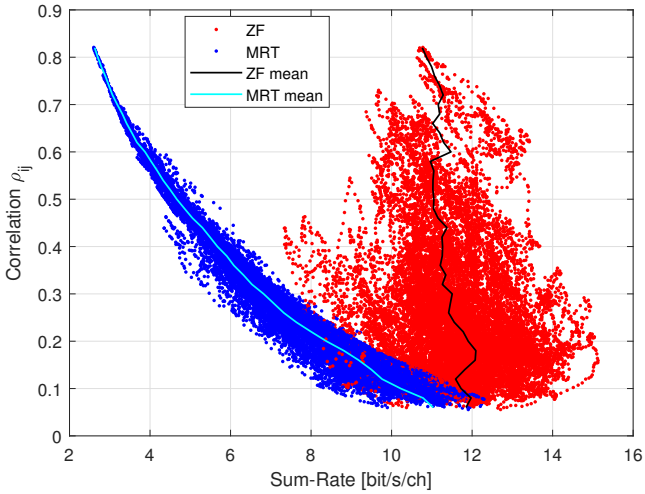

Fig. 4. Precoding sum-rates vs correlation for 18 snapshot averaging (approximately 2 λ movement).

link and small variations from Fig. 4. The mean sum-rates have some local variations, but the larger trend is an increase in sum-rates with increase in inter-user distances. A linear fit indicates 0.081 increase in sum-rate per meter. Due to the curved relation between correlation and MRT sum-rate in Fig. 4, the difference between the percentile curves is more constant in Fig. 5 compared to Fig. 2.

MRT sum-rates are plotted against MB_Δ in Fig. 6, and again the strong link between MRT sum-rates and correlation is obvious when comparing the mean sum-rate and correlation between figures 3 and 6. The sum-rate vs inter-user distance for the ZF precoder is shown in Fig. 7 where the trend for mean sum-rate is almost flat across inter-user distances, with a 0.0031 increase in sum-rate per meter. This is not unexpexted when considering the low dependency between correlation and sum-rate for ZF shown in Fig. 4.

The correlation, MB_Δ (beam scanning) and sum-rates where also calculated based on more snapshots to test if there was any major differences or small scale fading impacting the results. Averages over 9, 18 and 27 snapshots where used

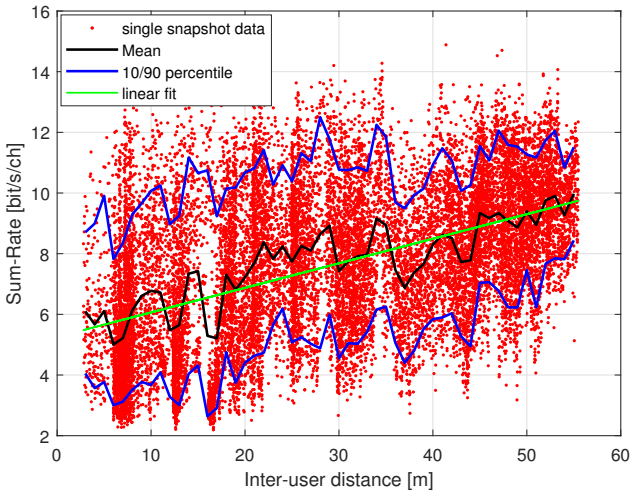

Fig. 5. Inter-user distance vs MRT sum-rate.

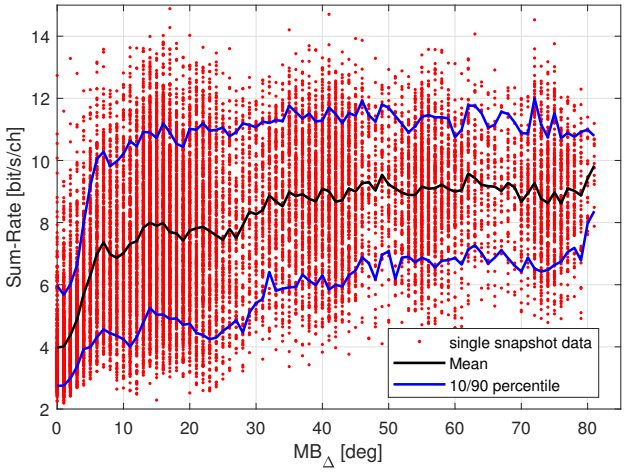

Fig. 6. Main beam directional separation vs MRT sum-rates.

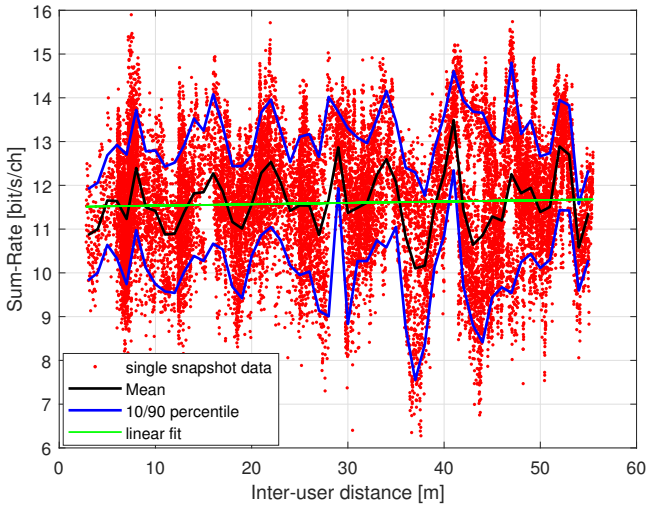

Fig. 7. Inter-user distance vs ZF sum-rates.

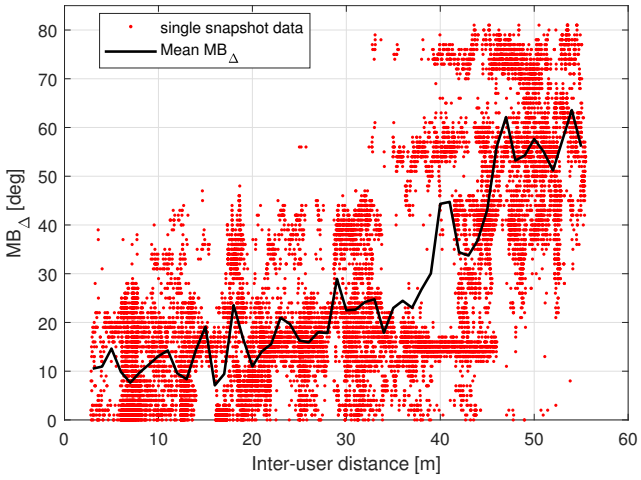

Fig. 8. Inter-user distance vs Main beam directional separation.

which corresponds to approximately 1, 2 and 3 wavelengths of movement. The averaged results shows correlation and sum-rates are more compressed as the highest and lowest values disappear with higher averaging. The shape of the point "clouds" stay similar and the mean is very similar for all averaging levels, with just minor deviations around the single snapshot mean shown in the paper.

In Fig. 8 the inter-user distance is plotted against the MB_Δ. The plot appears to have two distinctly different regions, where the first 35 meters of inter-user distance is very different from the remaining part of the plot. This two part plot is likely caused by the geometry of the measurement area and the location of the measurement tracks. The most dramatic drop in MRT sum-rate was seen for the MB_Δ below about 15°, and this range of low angular separation can be observed across a large range of inter-user distances in Fig. 8. This indicates that the MB_Δ and the user distance is not strongly linked.

V. Conclusion

For a NLOS scenario with relatively close distance from users to base station, correlation and sum-rate capcity was compared to distance and angular separation of users for MRT and ZF precoding. The mean correlation is found to be directly linked to inter-user distance and main beam separation. The link to distance is relatively slow at a rate of 0.0064 per meter. The MB_Δ impacts the correlation heavily by a 0.35 change in correlation from 0 to 15°, and minor change of 0.1 for the range of 15 to about 75°. The number of BS elements to user ratio of 8:1 is sufficient for ZF to not be heavily impacted by correlation or distances, while the MRT precoder is directly impacted by the correlation. The correlation is consistently but slowly changing with inter-user distance, but is heavily impacted by low angular separation of main beams. These results in NLOS scenario suggest that a distance criteria alone is not sufficient to accurately model the level of correlation or cluster sharing in channel models.

Acknowledgment

The authors would like to thank Huawei Sweden AB for their financial support.

REFERENCES

[1] F. Boccardi, R. W. Heath, A. Lozano, T. L. Marzetta, and P. Popovski, "Five disruptive technology directions for 5g," *IEEE Communications Magazine*, vol. 52, no. 2, pp. 74–80, February 2014.

[2] F. Rusek, D. Persson, B. K. Lau, E. G. Larsson, T. L. Marzetta, O. Edfors, and F. Tufvesson, "Scaling up mimo: Opportunities and challenges with very large arrays," *IEEE Signal Processing Magazine*, vol. 30, no. 1, pp. 40–60, Jan 2013.

[3] E. G. Larsson, O. Edfors, F. Tufvesson, and T. L. Marzetta, "Massive MIMO for next generation wireless systems," *IEEE Communications Magazine*, vol. 52, no. 2, pp. 186–195, February 2014.

[4] T. L. Marzetta, "Noncooperative cellular wireless with unlimited numbers of base station antennas," *IEEE Transactions on Wireless Communications*, vol. 9, no. 11, pp. 3590–3600, November 2010.

[5] H. Q. Ngo, E. G. Larsson, and T. L. Marzetta, "Aspects of favorable propagation in massive mimo," in *2014 22nd European Signal Processing Conference (EUSIPCO)*, Sep. 2014, pp. 76–80.

[6] S. Payami and F. Tufvesson, "Channel measurements and analysis for very large array systems at 2.6 ghz," in *2012 6th European Conference on Antennas and Propagation (EUCAP)*, March 2012, pp. 433–437.

[7] X. Gao, F. Tufvesson, O. Edfors, and F. Rusek, "Measured propagation characteristics for very-large mimo at 2.6 ghz," in *2012 Conference Record of the Forty Sixth Asilomar Conference on Signals, Systems and Computers (ASILOMAR)*, Nov 2012, pp. 295–299.

[8] À. O. Martínez, E. D. Carvalho, and J. Ø. Nielsen, "Towards very large aperture massive MIMO: A measurement based study," in *2014 IEEE Globecom Workshops (GC Wkshps)*, Dec 2014, pp. 281–286.

[9] Chen-Nee Chuah, D. N. C. Tse, J. M. Kahn, and R. A. Valenzuela, "Capacity scaling in mimo wireless systems under correlated fading," *IEEE Transactions on Information Theory*, vol. 48, no. 3, pp. 637–650, March 2002.

[10] Da-Shan Shiu, G. J. Foschini, M. J. Gans, and J. M. Kahn, "Fading correlation and its effect on the capacity of multielement antenna systems," *IEEE Transactions on Communications*, vol. 48, no. 3, pp. 502–513, March 2000.

[11] À. O. Martínez, P. Eggers, and E. D. Carvalho, "Geometry-based stochastic channel models for 5G: Extending key features for massive MIMO," in *2016 IEEE 27th Annual International Symposium on Personal, Indoor, and Mobile Radio Communications (PIMRC)*, Sept 2016, pp. 1–6.

[12] L. Liu, C. Oestges, J. Poutanen, K. Haneda, P. Vainikainen, F. Quitin, F. Tufvesson, and P. D. Doncker, "The cost 2100 mimo channel model," *IEEE Wireless Communications*, vol. 19, no. 6, pp. 92–99, December 2012.

[13] Styrelsen for Dataforsyning og Effektivisering. (2019) Grundlæggende landkortdata. [Online]. Available: https://kortforsyningen.dk/indhold/english

[14] S. Zhang, T. L. Jensen, O. Franek, P. C. F. Eggers, C. Byskov, and G. F. Pedersen, "Investigation of a UWB wind turbine blade deflection sensing system with a tip antenna inside a blade," *IEEE Sensors Journal*, no. 22, pp. 7892–7902, Nov 2016.

[15] J. Ø. Nielsen, W. Fan, P. C. F. Eggers, and G. F. Pedersen, "A channel sounder for massive mimo and mmwave channels," *IEEE Communications Magazine*, vol. 56, no. 12, pp. 67–73, December 2018.

[16] H. Krim and M. Viberg, "Two decades of array signal processing research: the parametric approach," *IEEE Signal Processing Magazine*, vol. 13, no. 4, pp. 67–94, July 1996.

[17] E. Björnson, M. Bengtsson, and B. Ottersten, "Optimal multiuser transmit beamforming: A difficult problem with a simple solution structure [lecture notes]," *IEEE Signal Processing Magazine*, vol. 31, no. 4, pp. 142–148, July 2014.

[18] E. Björnson and E. J. and, *Optimal Resource Allocation in Coordinated Multi-Cell Systems*. now, 2013. [Online]. Available: https://ieeexplore.ieee.org/document/8187586

[19] E. Björnson, M. Bengtsson, and B. Ottersten, "Optimal beamforming," https://github.com/emilbjornson/optimal-beamforming .

[20] P. Harris, W. Boukley Hasan, L. Liu, S. Malkowsky, M. Beach, S. Armour, F. Tufvesson, and O. Edfors, "Achievable rates and training overheads for a measured los massive mimo channel," *IEEE Wireless Communications Letters*, vol. 7, no. 4, pp. 594–597, Aug 2018.